Shaping of ultraviolet femtosecond laser pulses by Fourier domain harmonic generation

E Hertz, F Billard, G Karras, P Béjot, B Lavorel, O Faucher

Shaping of ultraviolet femtosecond laser pulses by Fourier domain harmonic generation

E. HERTZ,* F. BILLARD, G. KARRAS, P. BÉJOT, B. LAVOREL, AND O. FAUCHER

Laboratoire Interdisciplinaire Carnot de Bourgogne, UMR CNRS 6303 - Université Bourgogne Franche-Comté, 21078 Dijon Cedex, France
**edouard.hertz@u-bourgogne.fr*

Abstract: We present a method to finely tailor ultraviolet femtosecond laser pulses using a pulse shaper with ability in the infrared/visible spectral range. We have developed to that end a frequency doubling module in which the up-conversion mechanism is carried out in the Fourier plane of a $4f$-line. The pulse shaper is used to imprint a spectral phase and/or amplitude onto the fundamental pulse. The shaped pulse is then frequency doubled through the module which transfers the applied spectral shaping to the second harmonic field in a predictable manner. The relevance of the method is demonstrated by synthesizing and characterizing shaped pulses at a central wavelength of 400 nm. The results demonstrate a full control over the spectral phase and amplitude of the harmonic field. The experimental setup is simple and features interesting prospects for the polarization shaping of ultraviolet pulses and the production of shaped ultraviolet pulses requested for the seeding of free-electron lasers.

OCIS codes: (320.0320) Ultrafast optics; (320.5540) Pulse shaping; (320.7110) Ultrafast nonlinear optics.

References and links

1. A. M. Weiner, "Ultrafast optical pulse shaping: A tutorial review," Opt. Commun. **284**, 3669–3692 (2011).
2. A. M. Weiner, "Femtosecond pulse shaping using spatial light modulators," Rev. Sci. Instrum. **71**, 1929–1960 (2000).
3. J. Yang, F. Sakai, T. Yanagida, M. Yorozu, Y. Okada, K. Takasago, A. Endo, A. Yada, and M. Washio, "Low-emittance electron-beam generation with laser pulse shaping in photocathode radio-frequency gun," J. Appl. Phys. **92**, 1608–1612 (2002)
4. M. B. Danailov, A. Demidovich, and R. Ivanov, "Design of a two-stage laser pulse shaping system for FEL photoinjectors," Proc. 28^{th} FEL Conf. 617–620 (2006).
5. F. Calegari, D. Ayuso, A. Trabattoni, L. Belshaw, S. De Camillis, S. Anumula, F. Frassetto, L. Poletto, A. Palacios, P. Decleva, J. B. Greenwood, F. Martin, and M. Nisoli, "Ultrafast electron dynamics in phenylalanine initiated by attosecond pulses," Science **346**, 336–339 (2014)
6. T. Tanigawa, Y. Sakakibara, S. Fang, T. Sekikawa, and M. Yamashita, "Spatial light modulator of 648 pixels with liquid crystal transparent from ultraviolet to near-infrared and its chirp compensation application," Opt. Lett. **34**, 1696–1698 (2009).
7. B. J. Pearson and T. C. Weinacht, "Shaped ultrafast laser pulses in the deep ultraviolet," Opt. Express **15**, 4385–4388 (2007).
8. F. Verluise, V. Laude, Z. Cheng, Ch. Spielmann, and P. Tournois, "Amplitude and phase control of ultrashort pulses by use of an acousto-optic programmable dispersive filter: pulse compression and shaping," Opt. Lett. **25**, 575 (2000)
9. M. Hacker, G. Stobrawa, R. Sauerbrey, T. Buckup, M. Motzkus, M. Wildenhain, and A. Gehner, "Micromirror slm for femtosecond pulse shaping in the ultraviolet," Appl. Phys. B **76**, 711–714 (2003).
10. A. Rondi, J. Extermann, L. Bonacina, S. M. Weber, and J.-P. Wolf, "Characterization of a mems-based pulse-shaping device in the deep ultraviolet," Appl. Phys. B **96**, 757–761 (2009).
11. D. S. N. Parker, A. D. G. Nunn, R. S. Minns, and H. H. Fielding, "Frequency doubling and fourier domain shaping the output of a femtosecond optical parametric amplifier: easy access to tuneable femtosecond pulse shapes in the deep ultraviolet," Appl. Phys. B **94**, 181–186 (2009).
12. M. Hacker, R. Netz, M. Roth, G. Stobrawa, T. Feurer, and R. Sauerbrey, "Frequency doubling of phase-modulated, ultrashort laser pulses," Appl. Phys. B **73**, 273–277 (2001).
13. M. Hacker, T. Feurer, R. Sauerbrey, T. Lucza, and G. Szabo, "Programmable femtosecond laser pulses in the ultraviolet," J. Opt. Soc. Am. B **18**, 866–871 (2001).
14. H. Wang and A. M. Weiner, "A femtosecond waveform transfer technique using type II second harmonic generation," IEEE J. Quantum Electron. **40**, 937–945 (July 2004).

15. S. Shimizu, Y. Nabekawa, M. Obara, and K. Midorikawa, "Spectral phase transfer for indirect phase control of sub-20-fs deep uv pulses," Opt. Express **13**, 6345–6353 (2005).
16. C. Schriever, S. Lochbrunner, M. Optiz, and E. Riedle, "19 fs shaped ultraviolet pulses," Opt. Lett. **31**, 543–545 (2006).
17. P. Nuernberger, G. Vogt, R. Selle, S. Fechner, T. Brixner, and G. Gerber, "Generation of shaped ultraviolet pulses at the third harmonic of titanium-sapphire femtosecond laser radiation," Appl. Phys. B **88**, 519–526 (2007).
18. B. E. Schmidt, N. Thiré, M. Boivin, A. Laramée, F. Poitras, G. Lebrun, T. Ozaki, H. Ibrahim, and F. Légaré, "Frequency domain optical parametric amplification," Nat Commun **5**, 1–8 (2014).
19. S. Cialdi and I. Boscolo, "A laser pulse shaper for the low-emittance radiofrequency SPARC electron gun," Nucl. Instr. Meth. Phys. Res. **526**, 239–248 (2004)
20. K. A. Walowicz, I. Pastirk, V. V. Lozovoy, and M. Dantus, "Multiphoton intrapulse interference. 1. control of multiphoton processes in condensed phases," J. Phys. Chem. A **106**, 9369–9373 (2002).
21. M. Comstock, V. V. Lozovoy, I. Pastirk, and M. Dantus, "Multiphoton intrapulse interference 6; binary phase shaping," Opt. Express **12**, 1061–1066 (2004).
22. A. Monmayrant, S. Weber, and B. Chatel, "A newcomer's guide to ultrashort pulse shaping and characterization," J. Phys. B: Atomic, Molecular and Optical Physics **43**, 103001 (2010).
23. J. C. Vaughan, T. Feurer, K. W. Stone, and K. A. Nelson, "Analysis of replica pulses in femtosecond pulse shaping with pixelated devices," Opt. Express **14**, 1314–1328 (2006).
24. F. Frei, A. Galler, and T. Feurer, "Space-time coupling in femtosecond pulse shaping and its effects on coherent control," J. Chem. Phys. **130**, 034302 (2009).
25. M. M. Wefers and K. A. Nelson, "Space-time profiles of shaped ultrafast optical waveforms," IEEE J. Quantum Electron. **32**, 161–172 (Jan 1996).
26. R. Thurston, J. Heritage, A. Weiner, and W. Tomlinson, "Analysis of picosecond pulse shape synthesis by spectral masking in a grating pulse compressor," IEEE J. Quantum Electron. **22**, 682–696 (1986).
27. R.Selle, P. Nuernberger, F. Langhojer, F. Dimler, S. Fechner, G. Gerber, and T. Brixner,"Generation of polarization-shaped ultraviolet femtosecond pulses," Opt. Lett. **33**, 803-805 (2008)

1. Introduction

Programmable temporal shaping of femtosecond (fs) pulses has resulted in major advances in a wide array of physics with plenty of breakthrough applications for controlling atoms or molecules, pulse compression, and nonlinear microscopy to name a few. [1] All techniques enabling the generation of sophisticated optical waveforms operate in the frequency domain. By controlling the spectral phase and amplitude of the electric field, nearly any arbitrary pulse shape can be synthesized. So far, the most popular modulator uses a spatial light modulator based on liquid crystal (SLM-LC) inserted within a $4f$ line. An alternative method makes use of acousto-optical modulator (AOM). [2] Conventional pulse shapers have been predominantly developed in the visible (VIS) and near infrared (NIR) spectral domain because of the limited transparency range of implemented materials. This property was in addition compatible with the most widely used fs laser source, namely the Ti:sapphire operating in the near-infrared. The availability of shaped pulses in the ultraviolet (UV) spectral domain is nevertheless of utmost importance. For instance, many organic systems have their absorption bands in this spectral range. Most of investigations on this topic have been therefore based on multiphoton excitation with IR fields which excludes *de facto* the possibility of weak field excitation. This strategy prevents also a control over the phase of the excitation without modifying the transition probability which sometimes implies the use of tricky normalization procedures. Temporal shaping of UV pulses represents also a major challenge regarding free electron lasers (FELs). A uniform temporal electron bunch reduces the beam emittance by minimizing the nonlinear space charge effects in the photoelectrons pulse. As a result, the optimal pulses for the excitation of the photocathode must have flat-top shape of few picosecond (ps) duration in the UV range. [3,4] Finally, another potential application of UV shaping is the "upcoming" field of attochemistry, where shaped UV pulses could be used in order to control the fate of the excited cationic states produced by the extreme ultraviolet pulses. [5]

Despite numerous applications, commercially available devices operating in the UV spectral range are still very limited and feature several limitations. Apart from specific laboratory developments [6] or prototypes proposed by few companies, the SLM-LC presents absorption

in UV that causes photochemical damage. Specific models of acousto-optical modulators [7] or acousto-optic programmable dispersive filter (AOPDF) [8] enable operation in the UV range down to about 250 nm. However, the output energy is often limited due to the low conversion efficiency or damage threshold. A different approach based on deformable mirrors or micro electro mechanical system (MEMS) offers, with a suitable coating, extension to the UV range. [9, 10] Nevertheless, they do not allow for gray-level control of the spectral amplitude and shaping by deformable mirror is also limited to smoothed phase functions of moderate amplitude.

All these devices are not yet in widespread use in laboratory research compared to the common NIR/VIS SLM-LC. As a result, there is still a strong demand for simple and low-cost alternatives enabling temporal shaping of UV pulses from already available modulators, namely for methods converting shaped waveforms produced in the NIR/VIS to new wavelength. In this issue, different strategies of "indirect shaping" have been proposed. One of them is based on the second harmonic generation (SHG) of a shaped pulse [11, 12] but the conversion efficiency depends on the pulse shape and the prediction of the shaping to apply is complicated as discussed in section 2. Another scheme largely investigated relies on type II SHG or sum-frequency mixing (SFM) between a shaped pulse and another chirped pulse covering the time window of the shaped pulse. [13–17] SFM method features nevertheless several issues like the resulting chirp of the shaped UV pulse as well as the group delay mismatch between the generated UV and input VIS/NIR pulses which imposes special care. [13, 15]

We investigate here an alternative method for converting NIR/VIS shaped waveforms to the UV spectral range. The approach is still based on frequency doubling of a shaped pulse but the key idea is to carry out the latter in the Fourier plane of a $4f$-line. Such a strategy has been recently applied for a frequency-domain parametric amplification of single-cycle laser pulses. [18] A SHG module described in section 3 has been developed to this end. This module, suitably designed for having a net zero-dispersion of the output UV pulse, has been located at the exit of a standard SLM-LC shaper enabling spectral phase and amplitude modulation of NIR/VIS pulses. To illustrate the ability of the strategy, we have applied several useful modulations and characterized both IR (800nm) and UV (400 nm) fields in the frequency and time domain by spectral interferometry and cross-correlation, respectively. The results detailed in section 4 reveal a full control over the spectral phase and amplitude through a predictable and straightforward transfer of the applied shaping. The experimental device is compact, simple and overcomes most of the limitations of the current devices. The module operates with amplified laser pulses and the output UV energy can be large enough to induce nonlinear excitation or to deliver reasonable peak power when large temporal broadening is needed like in FEL photoinjectors. [19] The tunability in wavelength of the tailored pulse can be obtained by shaping a pulse provided by an optical parametric amplifier. The waveform distortions are assessed in section 5 and found comparable with the ones encountered with common SLMs. Finally, the method is easily implementable with a feedback loop optimization procedure.

2. Principle

The purpose of the present work is to tailor UV fs pulses using a pulse shaper operating in the infrared/visible spectral range. The pulse shaper modulates the spectral phase and/or amplitude of a pulse that is further frequency doubled through a procedure insuring a well defined transfer of the applied shaping onto second harmonic field. Suppose that the spectrum of the field after the pulse shaper is written as:

$$E(\nu) = \varepsilon(\nu)e^{i\varphi(\nu)}, \tag{1}$$

where φ and ε denote the spectral phase and amplitude of the pulse at the fundamental frequency, respectively. Assuming that this pulse is directly frequency doubled using a type I doubling

crystal, the harmonic field would be given by:

$$E_2(2\nu) \propto \int_{-\infty}^{+\infty} \varepsilon(\nu+\nu')e^{i\varphi(\nu+\nu')}\varepsilon(\nu-\nu')e^{i\varphi(\nu-\nu')}d\nu', \tag{2}$$

where the subscript "2" refers to the SHG radiation throughout the manuscript. As shown by this formula, the SHG field produced at a given frequency 2ν results from a sum over all spectral components of the fundamental field that add up to this frequency. This mixing of frequency components within the spectrum affects both spectral phase and amplitude. This effect can be exploited in order to control multiphoton process [20] by taking advantage of the interferences associated with the phase of each frequency component that contributes to the nonlinear excitation. For the present purpose, this effect is detrimental. The intricate interplay between spectral phase and amplitude in the SHG spectrum limits the shaping extent. This strategy does not provide a full control over the spectral phase and amplitude, and prevents for instance pure phase shaping of harmonic fields, i.e. control at constant energy. Any phase modulation of the fundamental field will indeed result in a modification of the second harmonic amplitude (with possible modifications of the spectral shape). Finally, regarding the complexity of Eq. (2), it is difficult to identify the modulation that should be imprinted on the fundamental field in order to reach (when possible) or to best suit the desired shaping after frequency up-conversion. As a result, a feedback from the experiment can be required to obtain the desired harmonic shaped pulse. [21] Ideally, each frequency component should be mixed only with itself in order to get rid of the crossing of the frequency components. Based on this idea, the approach proposed here consists in doubling the frequency of a shaped pulse in the Fourier plane of a $4f$ line. In this case, the fundamental field in the Fourier plane can be written as:

$$E(\nu, x) = E(\nu)e^{\left(\frac{x-\alpha\nu}{\omega_0}\right)^2}, \tag{3}$$

where x is the coordinate along which the frequencies are spread, α the spatial dispersion and ω_0 the beam waist of each frequency component. The central frequency versus x is given by $\nu(x) = x/\alpha$. If we assume, to first order, an "infinite" spectral resolution so that $\omega_0 \to 0$ in the previous equation, then:

$$E(\nu, x) = E(\nu)\delta(\nu - \nu(x)), \tag{4}$$

where δ is the Dirac delta function. In this case, only a single frequency component is found at a given point x. The integration in Eq. (2) becomes a simple product and the relationship between fundamental and SHG spectrum is greatly simplified since:

$$E_2(2\nu) \propto E^2(\nu) = \varepsilon^2(\nu)e^{2i\varphi(\nu)}, \tag{5}$$

so that the spectral amplitude ε_2 and phase φ_2 of the harmonic field writes as:

$$\varepsilon_2(\nu) = \varepsilon^2(\nu/2) \tag{6}$$

$$\varphi_2(\nu) = 2 \times \varphi(\nu/2). \tag{7}$$

The transcription of the initial shaping towards the SHG field relies now on a simple and clear transfer function where phase and amplitude modulation are entirely decorrelated. The method provides therefore the possibility of applying pure phase modulations. Shaping of great extent, versatility and high degree of control is therefore expected through this procedure. One question relies on the spectral bandwidth of the harmonic field provided by this unusual SHG scheme. Actually, for a Gaussian IR spectrum, it turns out to be the same as the one obtained through a direct doubling (Eq. (2)) of the Fourier Transform Limited (FTL) pulse.

3. Experimental set-up

In the present experiment, the fundamental IR pulse is produced by a Ti:sapphire chirped pulse amplifier that delivers pulses of 110 fs duration, centered around 800 nm, at 1 KHz repetition rate. The pulse is first shaped with a programmable $4f$ pulse shaper. The latter is composed of a pair of diffraction gratings (1600 grooves/mm) and a pair of cylindrical mirrors (400 mm focal length) arranged in a zero-dispersion line. A configuration using a vertical tilt of the optical components is adopted for limiting the geometrical aberrations. A programmable one-dimensional dual mask LC-SLM array (SLM-320d from Jenoptik) is placed at the Fourier plane of the pulse shaper. This SLM allows for independent control of the spectral phase and amplitude. We have calibrated the dispersion of the pulse shaper in the Fourier plane. From this measurement, we can deduce the averaged value of the spectral sampling $\overline{\Delta\nu_{\text{IR}}}$ =6.05 10^{10} Hz/pix (it should be emphasized that the dispersion does not follow a strictly linear law).

The module developed for the frequency domain SHG, located at the exit of the LC-SLM is depicted in Fig. 1. It is also based on a $4f$ line configuration. The first grating G1

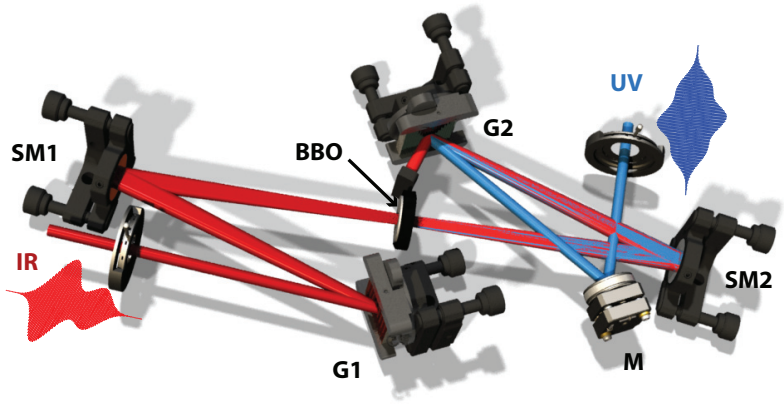

Fig. 1. SHG module. BBO: second-harmonic generation BBO crystal, SM1/SM2: IR/UV spherical mirror f=150 mm, G1: IR grating (1500 g/mm), G2: UV grating (3000 g/mm), M: flat mirror.

(1500 g/mm), set close to the Littrow angle, provides the angular dispersion of the frequency components contained within the IR pulse. The first mirror SM1 (f=150 mm) converts the angular dispersion to a spatial separation at the Fourier plane. Spherical mirrors (instead of cylindrical ones) are used in order to maximize the intensity at the Fourier plane where the SHG is produced. A type I BBO crystal with a thickness of 500 μm, placed at the Fourier plane, generates the SHG field. The IR is horizontally polarized while the UV is vertically polarized. A second spherical mirror SM2 identical to the first one focuses both IR and UV beams on the second grating G2. This grating must recombine the generated UV frequencies into a single collimated beam. In this issue, a grating G2 different from G1 must be used as a result of the wavelength change. This point is easily understood from the grating equation giving the relation between the incident angle θ_i and the diffracted angle θ_d:

$$\sin(\theta_i) + \sin(\theta_d) = \frac{m\lambda}{a}, \tag{8}$$

in which m is the order of diffraction (equal to one here), and a the groove spacing. In a conventional $4f$ line, the incident angle on the second grating is $\theta_d(\lambda)$, so that all the frequency components are diffracted in the same direction θ_i if the wavelength remains unchanged. In the

present case, the wavelength of interest is divided by two by the doubling process. This implies a reduction of the groove separation a by the same amount for having the UV components all diffracted under the same angle θ_i. A UV grating of 3000 grooves/mm has been therefore considered for G2 but as a general rule, the ratio λ/a should remain constant for the two gratings. With the present scheme, we obtain a net zero-dispersion line for the UV beam while the IR beam is diffracted in another direction without any need of spectral separation.

In the present approach, the SHG is produced in the Fourier plane of the device where the pulse is spatially and temporally stretched. As a result, one possible limitation of the method could be the low conversion efficiency $\mathcal{E}_{\mathrm{UV}}/\mathcal{E}_{\mathrm{IR}}$ where $\mathcal{E}_{\mathrm{IR}}$ and $\mathcal{E}_{\mathrm{UV}}$ stand for the energy before and after the doubling module, respectively. The conversion efficiency of the overall doubling module, which depends on the incident energy, reaches 12% for $\mathcal{E}_{\mathrm{IR}}$=140 μJ. The UV energy is therefore large enough for linear and possibly nonlinear excitation and more importantly remains constant when applying phase modulations with the pulse shaper as shown below. Moreover, to address the global efficiency of our technique, we emphasize that the transmission of the first stage (i.e. the pulse shaper) is 80% so that the typical energy before the pulse shaper remains attainable with current optical parametric amplifiers if wavelength tunability is needed.

In order to characterize the phase modulation imprinted onto the IR pulse, spectral interferometry measurement has been implemented. A part of the incident beam is selected before entering the pulse shaper to produce the reference pulse. The reference and shaped pulses are then sent into a spectrometer with a fixed delay. Analysis of the spectral fringes gives access to the spectral phase difference between the two pulses. [22] It should be pointed out that this method is not self-referenced and provides only the phase modulation introduced by the pulse shaper and not the absolute spectral phase of the pulse. It has been confirmed nonetheless that the initial pulse was FTL. Characterization in the time domain is achieved through intensimetric cross-correlation (CC) measurement. To that end, the reference and shaped beams are recombined and the two pulses copropagating with crossed polarizations are focused in a type II BBO crystal. The SHG signal is then detected as a function of the delay between the two pulses to provide the CC curve. Time and frequency domain characterizations of the UV pulse rely on the same principles. For the time domain, CC measurement is based on optical kerr effect. The IR reference pulse is recombined with the shaped UV pulse. The relative polarizations of the two fields are set at 45° and both pulses are focused in a thin glass plate. The depolarization of the UV pulse as a function the delay τ is measured providing a signal proportional to $\int I_{\mathrm{ref}}^2(t-\tau)I_{\mathrm{sh}}(t)\mathrm{d}t$ with I_{ref} and I_{sh} the reference and shaped pulses intensity, respectively. For the frequency domain characterization, the IR reference pulse is frequency doubled by a thin type I BBO crystal, recombined with the shaped UV pulses and sent into the spectrometer for spectral interferometry measurement.

4. Result

In order to test the device, a quadratic spectral phase (k''=5000 fs^2) has been first encoded on the fundamental pulse. The characterization of the IR shaped pulse by spectral interferometry is depicted in Figs. 2(a) and 2(b). The applied phase, relying on our SLM calibration, is depicted in dashed line in Fig. 2(b) and well agrees with our measurement. The shaped pulse is then frequency doubled through the SHG module. The output pulse has been also characterized by spectral interferometry and the result is shown in Figs. 2(c) and 2(d). First inspection reveals that the spectral phase of the UV field turns out to be quadratic as well. In order to assess the transcription of the initial shaping to the harmonic field, we have depicted the expected phase according to Eq. (7), i.e. $2\times\varphi(\nu/2)$, where $\varphi(\nu)$ corresponds to the phase measured for the fundamental field in Fig. 2(b). As observed, a relatively good agreement is found between the two curves in the spectral region of measurable intensity. Figure 2(c) depicts the UV spectral intensity $I_2(\nu)$ together with the expectation provided by Eq. (6), i.e. $I^2(\nu/2)$. Again a good

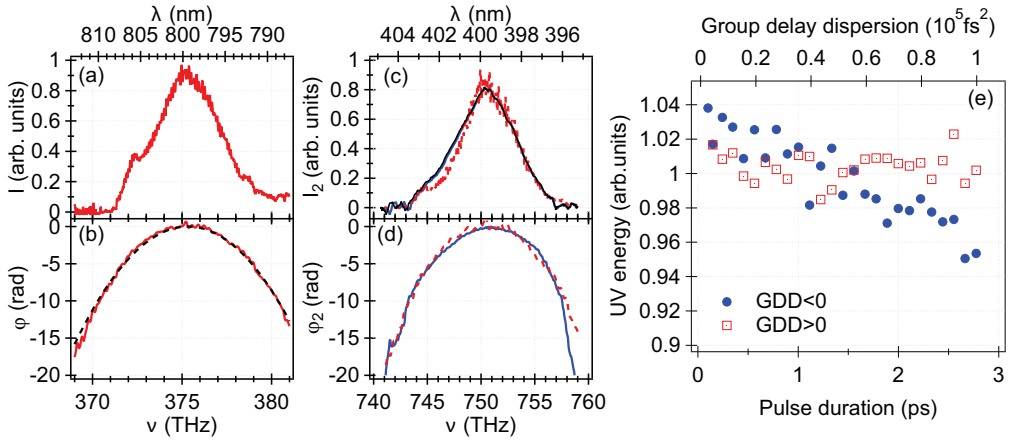

Fig. 2. Spectral interferometry measurement of fundamental (a,b) and SHG field (c,d) when applying a quadratic phase: (a) spectral intensity $I(\nu)$ of the fundamental field, (b) measured spectral phase $\varphi(\nu)$ (red solid line) compared to the applied phase (black dashed line), (c) spectral intensity $I_2(\nu)$ of SHG field (blue solid line) compared to $I^2(\nu/2)$ (red dashed line), (d) measured spectral phase $\varphi_2(\nu)$(blue solid line) compared to the expectation $2 \times \varphi(\nu/2)$ (red dashed line). (e) UV energy measured after the SHG module as a function of the group delay dispersion (GDD) applied to the fundamental field.

agreement is found confirming that the device faithfully transfers the applied shaping in a predictable way. We emphasize that the spectrum, along with the conversion efficiency $\mathcal{E}_{\mathrm{UV}}/\mathcal{E}_{\mathrm{IR}}$, remained unchanged when applying the quadratic phase compared to the unshaped pulse. This point is evidenced in Fig. 2(e) depicting the energy measured by a UV photodiode at the exit of the frequency doubling module for different amount of group delay dispersion applied to the fundamental field. As shown, the variation remains below 6% while the pulse duration is broadened up to 2.8 ps. It should be noted that the space time-coupling may contribute at least partially to the observed deviation.

The same procedure, with more complex phase modulations has been applied. Figure 3 displays off-centered phase step (a), sinusoidal modulation (b), phase gate (c), and triangular phase modulation (d). Again, the spectral phase of the UV field matches the theoretical expectation $2\times\varphi(\nu/2)$. Even for such complex phase modulations, the doubling module suitably transfers the phase information imprinted on the fundamental pulse. As for quadratic phase, we point out that the spectral amplitude was not affected when applying the different phases tested here, confirming the achievement of pure UV phase shaping at constant energy.

In addition, we have also characterized the pulses in the time domain. Figures 4(a,b) depict the cross-correlation of the IR and UV beams with the sinusoidal phase modulation of Fig. 3(b). As expected, the multiplication by a factor of 2 of the spectral phase through the doubling process (Eq. (7)) strongly modifies the pulse shape from IR to UV. This effect is properly reproduced by the calculation.

Finally, the ability of the module to apply a control over the spectral amplitude has also been verified. To that end, a sinusoidal modulation has been applied to the spectral amplitude of the IR pulse. Figure 5(a) depicts the spectral intensity of the IR field measured with and without modulation. From these curves, the modulation $M(\nu)$, defined as the ratio between the shaped and unshaped spectrum, is deduced and depicted in Fig. 5(b). Similar measurements performed for the UV pulse after the SHG module are presented in Figs. 5(c) and 5(d). According to Eq. (6), the modulation M_2 imprinted on the SHG field should follow the relationship $M_2(\nu) = M^2(\nu/2)$. This point is confirmed in Fig. 5(d).

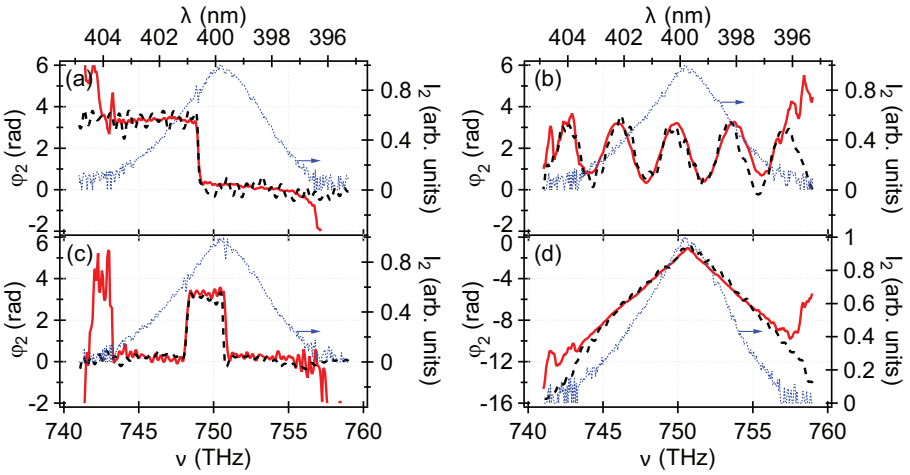

Fig. 3. Spectral interferometry characterization for various applied phases: phase step (a), sinusoidal phase modulation (b), phase gate (c), and triangular phase modulation (d). The spectral phases measured for the SHG field are shown in red solid lines. The black dashed lines depict the expectation $2 \times \varphi(\nu/2)$ where $\varphi(\nu)$ corresponds to the phase measured for the fundamental field. The spectral intensity $I_2(\nu)$ of SHG field is shown in blue dashed line in each panel.

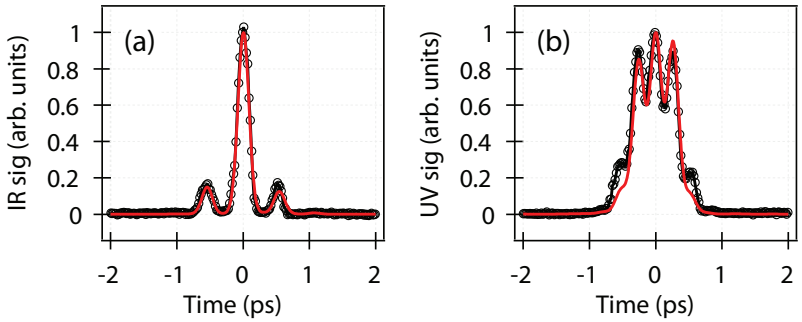

Fig. 4. Black lines with circle: cross correlation curve of IR (a) and UV (b) for the sinusoidal phase modulation of Fig. 3(b). The theoretical curves are shown in red color.

5. Evaluation of waveform distorsion

5.1. Temporal replica

The quality of the spectral phase transfer is not the only criteria to consider. Pulse shaping, especially with pixelated devices, are known to introduce a number of waveform distorsions and it is important to assess the behavior of the present frequency doubling module with respect to them. The major pulse distorsion of SLM-LCD concerns the replica related to the pixelated nature of the device whose effect can be understood through a simplified approach. [23] Assuming first a linear dispersion of the frequency on the Fourier plane and an infinite spectral resolution (equivalent to assume that the beam waist of each frequency component ω_0 tends to zero), the transfer function $H(\nu)$ can be written as:

$$H(\nu) = \sum_{n=1}^{n_{pix}} \mathrm{squ}\left(\frac{\nu - \nu_n}{\Delta\nu}\right) t_n e^{i\varphi_n}, \tag{9}$$

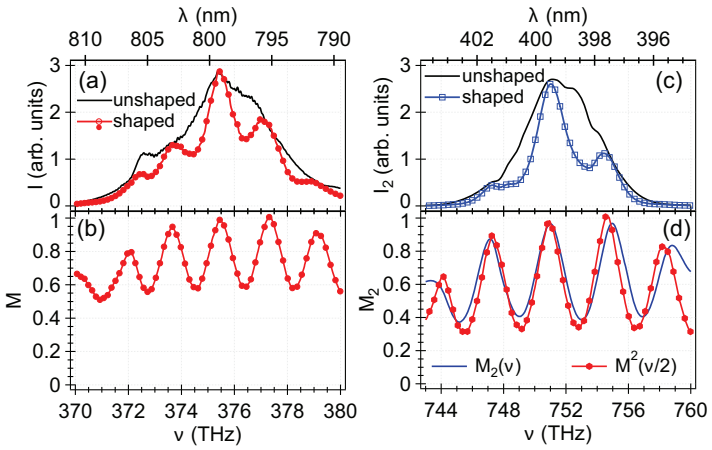

Fig. 5. Amplitude modulation by a sinus function. Unshaped and shaped IR spectra (a). Modulation $M(\nu)$ corresponding to the ratio between the shaped and unshaped spectrum (b). Unshaped and shaped UV spectra (c) and modulation $M_2(\nu)$ compared to the expectation $M^2(\nu/2)$ (d).

in which squ stands for the top-hat function, n is the pixel number, ν_n the central frequency of the nth pixel, and $\Delta\nu$ the frequency separation between the two sides of a pixel. t_n and φ_n represent the amplitude and phase modulation applied on the nth pixel respectively. If we assume now that the spectral amplitude of the field does not vary along a given pixel and is equal to E_n for the nth pixel, the Fourier transform provides the expression of the field in the time domain:

$$E(t) = \mathrm{sinc}(\pi\Delta\nu t) \sum_{n=1}^{n_{pix}} t_n E_n e^{i(2\pi\nu_n t+\varphi_n)}. \tag{10}$$

The term in the summation contains evenly-spaced frequency samples that induces replicas with a period $\Delta\tau = 1/\Delta\nu$ (the reciprocal of the frequency increment). With no applied modulation φ_n=cste, these replicas coincide with the zeros of the sinc function leaving the pulse unchanged. However, if a phase modulation shifts a part of the field at t≠0, the amplitude of the desired pulse will be reduced by the sinc function and replicas will appear. We will call hereafter replicas these undesired repetitions of the waveform. The origin of these replicas has been explained in a very simple way by Vaughan et al. [23] In the previous expression, φ_n corresponds to the desired phase. Because the applied phase is modulo 2π, this phase is indistinguishable from $\varphi_n + 2\pi Rn$ where R is an integer corresponding to the replica order. The desired pulse is obtained for $R = 0$. For $R \neq 0$ an additional linear spectral phase $2\pi Rn$ is added to the desired phase giving rise to time-delayed replica. According to Eq. (10), the replica should exhibit the same temporal shape as the desired pulse. In fact they are different as a result of the nonlinearity of the spectral dispersion (meaning that the additional phase is not purely linear).

These replica can be observed by applying linear phases to the IR pulse. We first apply a phase so as to induce a delay τ=6 ps on the IR beam. The cross-correlation measurement depicted in Fig. 6(a) shows the main pulse (M) time-delayed at τ=6 ps together with the first replica (R_1) which is broadened as a result of the nonlinear dispersion in the Fourier plane. The delay between the main pulse and the replica is $\Delta\tau_{IR}$ =16.5 ps in agreement with our measured spectral sampling of $\overline{\Delta\nu_{IR}}$=6.05 10^{10} Hz/pix. Figure 6(b) shows the cross correlation of the UV beam after passing through our frequency doubling module. It can be seen that the main UV pulse is

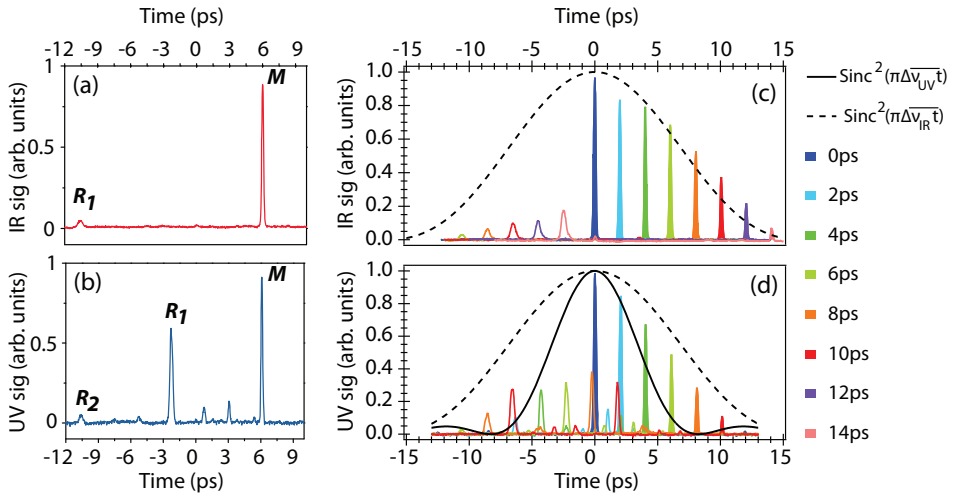

Fig. 6. (a) Cross-correlation measurement of the IR pulse for a linear phase inducing a delay τ=6 ps. *M* indicates the main (desired) pulse and R_1 the first replica. (b) Cross-correlation measurement of the UV pulse for the same phase, R_1 and R_2 refer to the first and second replica. In both measurement, the time origin is the position of the unshaped pulse. (c) IR and (d) UV experimental cross-correlation signal for various applied delays. Main pulses have been depicted with filled areas to better distinguish them from replica.

also delayed by 6 ps in spite of the up-frequency conversion. This is because both phase and spectral sampling are doubled via the doubling procedure so that the slope of the linear phase remains unchanged. The first UV replica R_1 is observed at $\tau = -2.25$ ps, corresponding to a separation with respect to the main pulse of $\Delta\tau_{UV}$=8.25 ps which is half of the delay observed for the IR pulse. As discussed previously, the delay between the main pulse and the replica is related to the spectral sampling. Because of the frequency doubling, we have $\overline{\Delta\nu_{UV}}=2\ \overline{\Delta\nu_{IR}}$ resulting in a separation $\Delta\tau_{UV}=\Delta\tau_{IR}/2$ which corroborates our observation. A second replica R_2 located at $2\Delta\tau_{UV}$ can even be observed. The other peaks can be attributed to the so-called wrap or modulator replica [23] related to the imperfections at the pixel edges. The applied phase is limited within a range of 2π so that the linear phase modulation will exhibit periodic abrupt phase wraps. These wraps in combination with the smoothed-out pixel regions create periodic distortions in the applied phase (compared to the theoretical linear phase) and therefore induce replica in the time domain. The periodicity of the wrap replicas that we have observed is in line with the relation $\Delta\tau_{wrap}=1/\Delta\nu_{wrap}$. The enhanced amplitude of these replica in the UV compared to the IR can be explained by the SHG process that leads to the doubling of the phase (see Eq. (7)) and therefore to the increase of the abrupt phase wraps amplitude. It can also be a signature of more pronounced pixel smoothing effect on the UV waveforms as a result of the doubling process. This assumption will be confirmed below.

In order to evaluate the achievable temporal window resulting from the sinc function in Eq. (10), a set of delays from 0 to 14 ps has been applied to the IR beam. The corresponding cross-correlation curves measurement, depicted in Fig. 6(c), shows the gradual decrease of the main pulse when the delay increases together with the appearance of the replica separated by $\Delta\tau_{IR}$. We have depicted in dashed lines the sinc time window, i.e. $\mathrm{sinc}^2(\pi\overline{\Delta\nu_{IR}}t)$ for our shaper. As observed, the measurement of variably delayed pulses follows roughly the sinc envelop. It should be noted that no spatial selection is applied on the output beam and that the focused configuration of the cross-correlation measurement limits the effect of additional time window by space-time coupling. Similar cross-correlation measurement have been conducted with the

produced UV shaped pulses and are depicted in Fig. 6(d). The expected sinc time windows corresponding to the UV and to the IR field are depicted in this figure (solid and dashed black line respectively). The measurement reveals that the delayed pulses do not follow the UV sinc time window but present a much slower decrease. This can be interpreted through a pixel edge smoothing effect occurring during the frequency doubling process. This effect, which can be detrimental as shown in Fig. 6(b) with the wrap replica, tends also to clean up the spectral shaping and allows here to better approach the ideal case of a linear phase modulation by a smoothing of the pixel shape. The result leads to an enhanced achievable time window ultimately quite close to the IR time window. In order to support this assessment, a simulation taking into account a smoothing of the phase $\varphi_2(\nu)$ has been performed and the result shown in Fig. 7 corroborates the observations. It should be noted that the effect of pixel edge smoothing could be limited by a tighter focusing of the spectral components in the UV module, i.e. using shorter focal length mirrors.

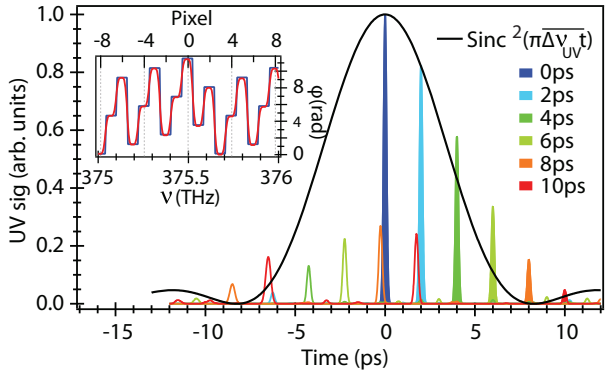

Fig. 7. Calculation of UV cross-correlation signal for various applied delay (to be compared with Fig. 6(d)) considering a smoothing of the phase. The inset shows the smoothed phase $\varphi_2(\nu)$ (red curve) together with the corresponding unsmoothed phase function (blue curve).

5.2. *Spatio-temporal coupling*

Another waveform distortion inherent to LC-SLM pulse shapers is the so-called spatio-temporal coupling. This effect is due to the spatial extension of the different spectral components in the Fourier plane (that has been neglected in Eq. (9)). The spatial profiles of the focused spectral components can be modified by the SLM and undergo different amounts of diffraction as a result of abrupt amplitude or phase steps on the modulator. The output field is therefore represented by a coupled function of space and time [1, 2] so that the transverse profile of the beam is modulated according to the temporal shaping. A simple analytical expression describing the space-time coupling has been reported by Wefers and Nelson. [25] Assuming an input electric field proportional to $f(x)E(t)$, and no aperture (or spatial filter) at the exit of the device, the electric field after the shaper writes as $E_{\text{out}}(t) = f(x + vt)E_{\text{sh}}(t)$ where $E_{\text{sh}}(t)$ is the temporal profile of the shaped pulse, x the transverse coordinate along the direction of the liquid crystal array and v the spatio-temporal coupling speed:

$$v = \frac{a\, c \cos\theta_i}{\lambda}, \tag{11}$$

in which c is the speed of light and a the groove spacing. As a result of the $f(x + vt)$ term in the output field, any time shift in the shaped waveform will be accompanied by a spatial shift along the transverse coordinate $\Delta x = -vt$. It should be pointed out that the use of an aperture

at the output would result in the occurrence of a time window. [26] We have evaluated the spatio-temporal coupling of our device by measuring, with a camera located at the exit of the set-up, the spatial shift of the beam for various programmed delays. In order to highlight the lateral shift, the input beam size has been reduced to about 1 mm. Figure 8(a) displays the IR beam spot with no modulation applied on the SLM, leading to the usual TEM_{00} mode. For a

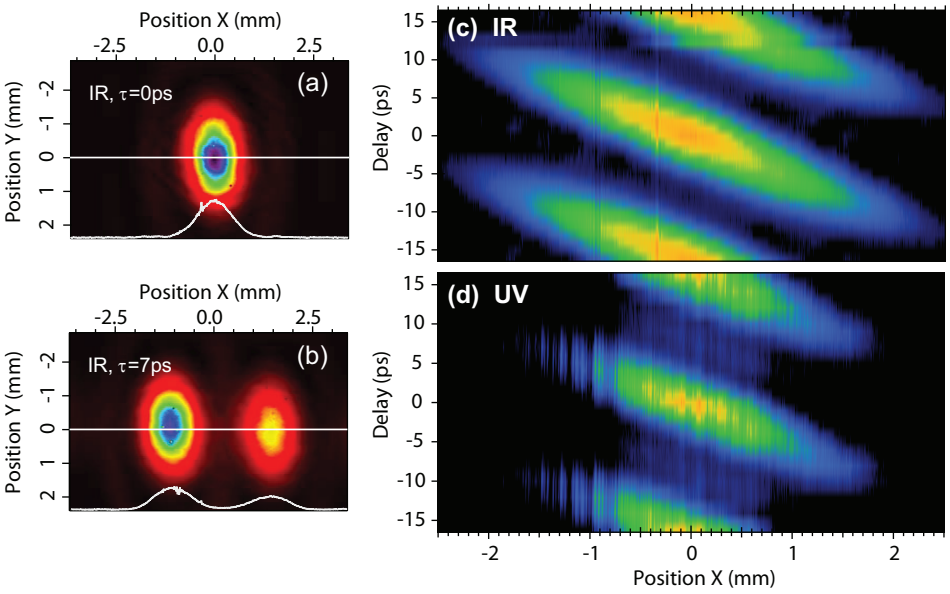

Fig. 8. IR transverse beam profile at the output of the pulse shaper with no modulation (a) and with a linear phase inducing a delay $\tau = 7$ ps (b). 1D beam profile, i.e. horizontal cut at $y = 0$, is depicted in white line on the bottom of each figure. IR (c) and UV (d) 1D beam profile recorded for various applied delays and compiled in a single picture (see text).

linear phase inducing a delay $\tau = 7$ ps, the output beam is split in two sub-spots associated with the main pulse and the replica [Fig. 8(b)]. The main pulse (delayed at $t > 0$) is shifted to the left while the replica ($t < 0$) is shifted to the right. On the bottom of each figure, the 1D beam profile corresponding to the horizontal cut at $y = 0$ is plotted in white line. This 1D beam profile has been recorded for various applied delays and the results compiled in Figs. 8(c) and 8(d) for the IR and UV beams respectively. In Fig. 8(c), one can see in the center of the figure the shift of the main pulse. As the delay increases, the beam moves along a line whose slope is defined by the spatio-temporal coupling speed. From the fit of these data, the speed is found to be $v \approx 150$ μm/ps in good agreement with the expectation provided by Eq. (11). The two symmetric beams observed up and down of Fig. 8(c) correspond to the replicas undergoing spatio-temporal coupling as well. The doubling module corresponds mainly to an additional $4f$-line, so that any initial shift of the beam should be preserved at the output. This effect is confirmed by the result of Fig. 8(d) depicting similar space-time coupling for the UV beam. The spatio-temporal coupling is not therefore amplified by the doubling module and remains moderate compared to the usual beam size of amplified laser systems. Furthermore, it should be mentioned that no space-time coupling is observed at the focal plane of a lens [24] so that it can be circumvented by conducting experiments with focused beams.

6. Conclusion

We have reported on the shaping of femtosecond UV pulses using a method converting waveforms from NIR to UV. The method is based on the SHG of tailored pulses synthesized in the NIR/VIS spectral range. The SHG is produced in the frequency domain, namely in the Fourier plane of a $4f$-line, by means of a frequency doubling module developed to that end. The device is simple, compact and enables a full control over the spectral phase and amplitude of the UV field. The performance of the set-up in term of reliability, energy conversion efficiency, or waveform distortions is of high quality and confirms the relevance of the method. The wavelength tunability can be obtained by shaping the output of an optical parametric amplifier that is further frequency doubled with the present module. The present module targets the broad community of pulse shaper users looking for an upgrade of their device providing an extension towards UV. The solution proposed here allows to reliably reach this objective with a low-cost and easily implementable set-up. Besides the potentialities highlighted in this paper, the device is also very promising for the generation of polarization-shaped fs UV laser pulses remaining out of reach with the current commercial devices. In this purpose, two perpendicularly orientated nonlinear crystals could be used in the Fourier plane in order to frequency double the spectral components of elliptical polarizations. [27] The two perpendicular components of the elliptic field could be therefore independently doubled with a transfer of their phase values.

Funding

Conseil Régional de Bourgogne (PARI program); CNRS; FEMTO network; Labex ACTION program (contract ANR-11-LABX-01-01); French National Research Agency (ANR) through the CoConicS program (Contract No. ANR-13-BS08-0013).